Supporting Information

Neelam et al. 10.1073/pnas.1502111112

SI Text

Estimate of Pressure Drop Across the Nuclear Membrane

The nuclear membrane contains nuclear pores and is permeable to water (1). Therefore, the net pressure drop across the nuclear membrane caused by the applied suction pressure P_s (Fig. S10*B*) is expected to drive flow out of the nucleus into the micropipette. Although this flow will, in principle, reduce the pressure drop across the membrane and thus the applied force, we show here that this reduction in force is negligible based on simple fluid mechanics considerations.

The volume flux across the membrane is given by

$$J_V = \varphi(P_0 - P_m), \quad \text{[S1]}$$

where P_0 is the hydrostatic pressure inside the nuclear membrane, P_m is the pressure outside the membrane, and φ is the filtration coefficient. Considering the resistance to fluid flow across the pores, φ can be estimated by (2)

$$\varphi = \frac{\rho \pi r^4}{8\mu l}, \quad \text{[S2]}$$

where ρ is density and μ is viscosity of the fluid, and r is radius and l is length of the nuclear pores. Assuming Poiseuille flow in the fluid-containing region of micropipette, the volume flux for radius R and fluid length L is

$$J_V = \varphi_p(P_m - P_s), \quad \text{[S3]}$$

where

$$\varphi_p = \frac{R^2}{8\mu L}\frac{3\lambda^3}{1+\lambda+\lambda^2}. \quad \text{[S4]}$$

Here, $\lambda = 1 + \frac{L}{R}\tan\theta$ for a tapered tube of angle θ. Equating the fluxes of the incompressible fluid yields

$$\frac{(P_0 - P_m)}{(P_0 - P_s)} = \frac{1}{1+\varphi/\varphi_p}. \quad \text{[S5]}$$

For typical literature values for nuclear pores (3, 4) (r = 3.5 nm, l = 50 nm, ρ = 5 μm^{-2}, R = 0.25 μm, L = 10 μm, θ=10°), we estimate the ratio in the denominator to be extremely small ($\varphi/\varphi_p < 10^{-5}$), making the right-hand side of Eq. **S5** close to unity. Therefore, the pressure at the outer membrane surface should be essentially equal to the suction pressure ($P_m \cong P_s$) for any reasonable range of membrane permeabilities and pipette dimensions, despite the existence of flow of fluid across the nuclear membrane.

1. Rowat AC, Lammerding J, Ipsen JH (2006) Mechanical properties of the cell nucleus and the effect of emerin deficiency. *Biophys J* 91(12):4649–4664.
2. Dahl KN, Kahn SM, Wilson KL, Discher DE (2004) The nuclear envelope lamina network has elasticity and a compressibility limit suggestive of a molecular shock absorber. *J Cell Sci* 117(Pt 20):4779–4786.
3. Mazzanti M, Bustamante JO, Oberleithner H (2001) Electrical dimension of the nuclear envelope. *Physiol Rev* 81(1):1–19.
4. Maeshima K, et al. (2010) Nuclear pore formation but not nuclear growth is governed by cyclin-dependent kinases (Cdks) during interphase. *Nat Struct Mol Biol* 17(9): 1065–1071.

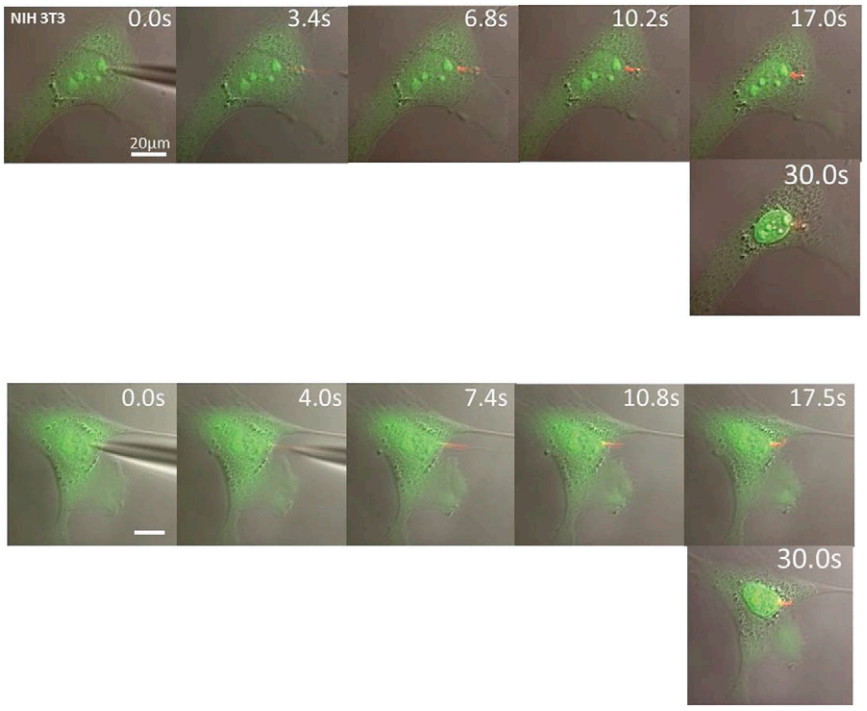

Fig. S1. Damage to the cell membrane is confined to a narrow tether while cells remain viable throughout the nuclear pulling. (*Top*) NIH 3T3 fibroblasts were incubated with the cell membrane-permeable green fluorescent nucleic acid dye SYTO 10 and the cell membrane-impermeable dye ethidium homodimer-2 (red), which diffuses into the cell only when there is significant membrane damage. On nuclear pulling, a narrow tether was observed to become red (3.4 s), suggesting cell membrane rupture. However, the leakage was confined to the tether alone because no red fluorescence was observed in the cytoplasm. The cell was observed not to turn red over a period of ∼30 s, suggesting that over the time scale of the experiment (10 s) the cell remains viable. In addition, no changes in cell morphology were observed during the micromanipulation. (*Bottom*) Another example of the same type of experiment.

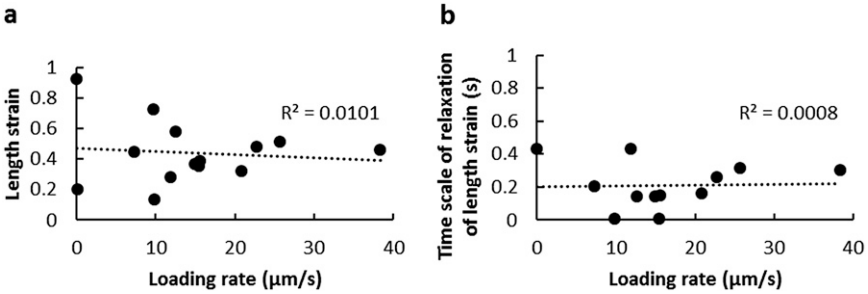

Fig. S2. Response of the nucleus is independent of the loading rate. Both the length strain (*A*) of the pulled nucleus just before detachment and the dynamics of length strain relaxation (*B*) were uncorrelated with the loading rate. The loading rate was computed from the slope of the distance traveled by the front edge of the nucleus versus time. The time scale for relaxation of the length strain was computed as shown in Fig. 2*B*.

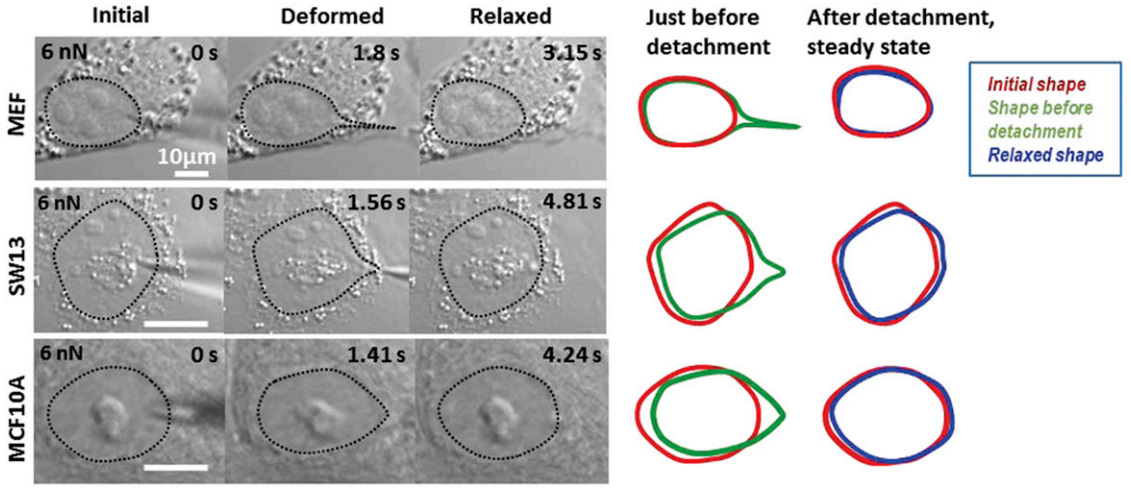

Fig. S3. Nuclear mechanics in other cell types. The formation of a nuclear protrusion under pulling forces, a much smaller translation of the back edge, followed by near complete nuclear relaxation was observed in a variety of cell types [MEFs, SW13 adrenal carcinoma cells, and human breast epithelial cells (MCF 10A cells)].

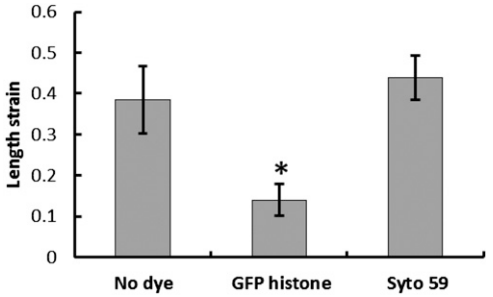

Fig. S4. Nuclear response does not change with SYTO 59 dye treatment. The length strain of the pulled nucleus just before detachment was quantified and found to be the same in unstained nuclei and nuclei stained with SYTO 59 dye, but significantly less in GFP-histone–labeled nuclei. $*P < 0.05$, $n = 10$.

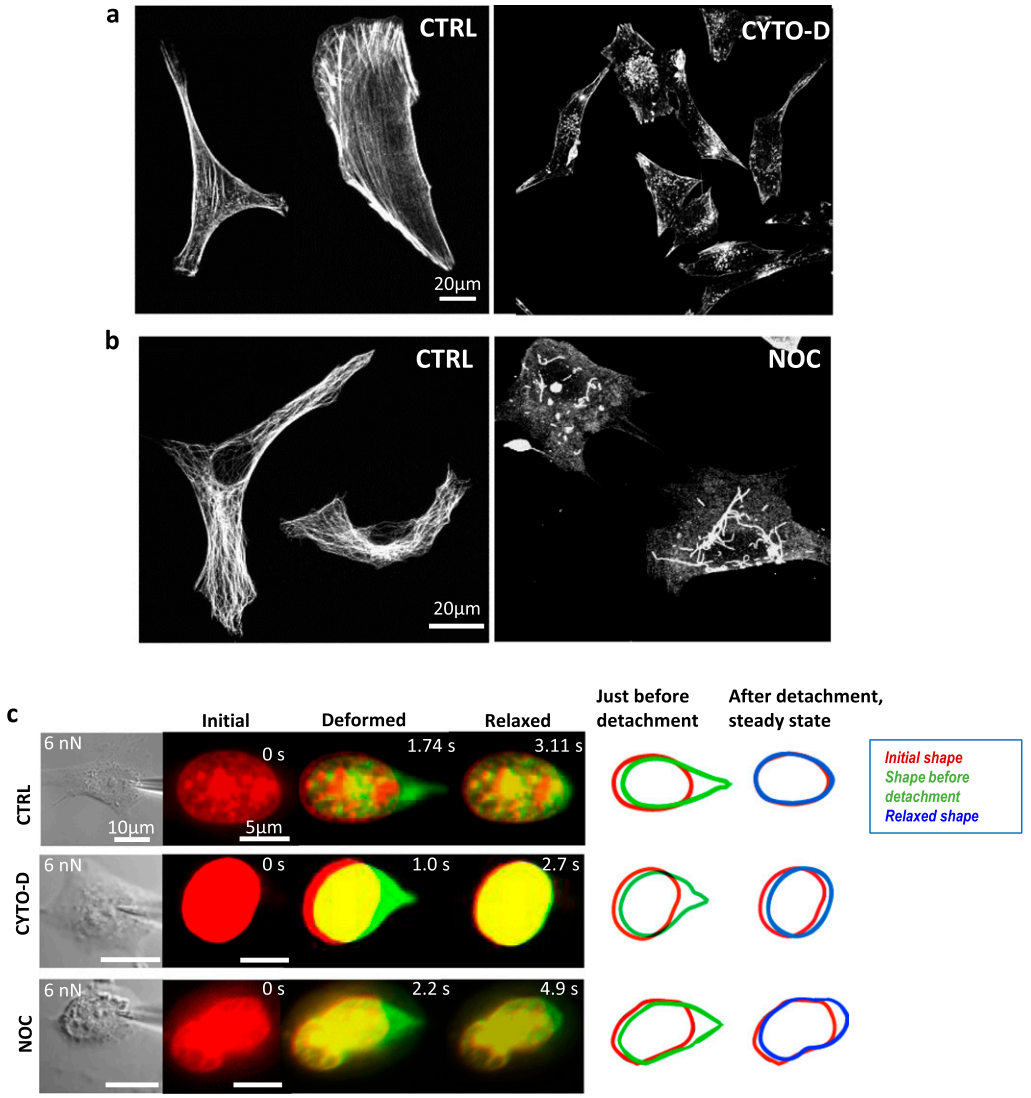

Fig. S5. F-actin and microtubule disruption in NIH 3T3 fibroblasts. (*A*) F-actin organized into actomyosin bundles in NIH 3T3 fibroblasts (CTRL), which were completely disrupted upon cytochalasin-D treatment (CYTO-D, 90 nM for 30 min). (*B*) Microtubule organization in normal (CTRL) and nocodazole-treated (NOC, 1 μM for 3 h) fibroblasts. Nocodazole treatment caused microtubules to look very short and fragmented. (*C*) Representative examples of the shapes of initial (red), deformed (green shape overlaid on the initial red shape), and relaxed (green relaxed shape overlaid with red initial shape) nuclei in control, F-actin–disrupted (CYTO-D–treated), and microtubule-disrupted (NOC-treated) NIH 3T3 fibroblasts. The overlaid outlines of the initial (red), pulled (green), and relaxed (blue) shapes are shown on the right.

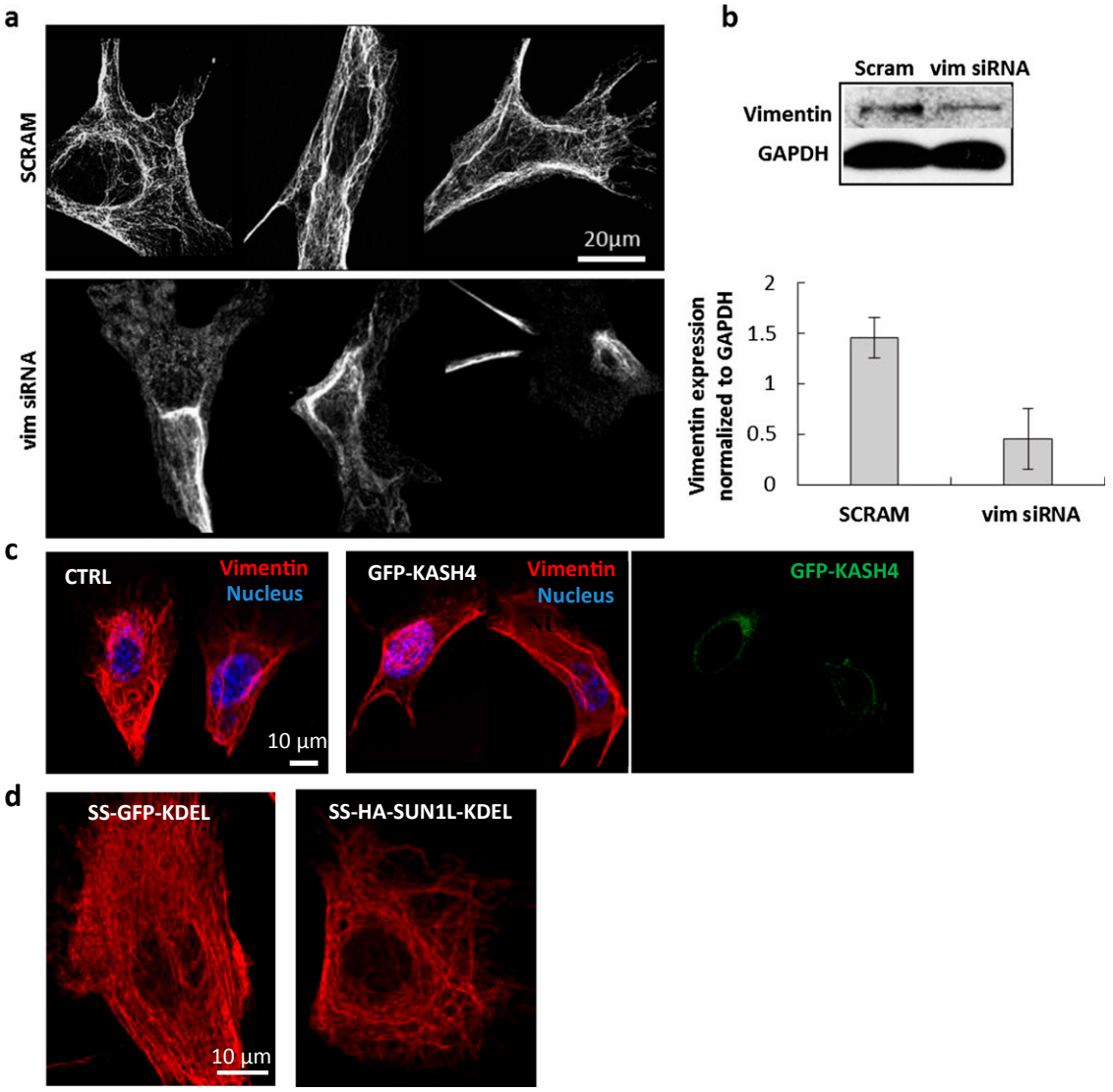

Fig. S6. Vimentin organization. (*A*) Well-organized VIFs are clearly visible in immunostained NIH 3T3 fibroblasts transfected with scrambled siRNA (SCRAM; three different examples are shown in the top panel; a "cage–like" structure can be observed in the cells). However, in cells transfected with vimentin siRNA (vim siRNA), filaments are far fewer, shorter, and disorganized. (*B*) Western blot showing vimentin and GAPDH (internal loading control) levels under the two conditions of SCRAM and vim-siRNA. Vimentin expression was compared by normalizing with GAPDH levels (plot below) showing a clear decrease in the expression. (*C*) Representative examples of vimentin intermediate filaments structure in NIH 3T3 fibroblasts (CTRL) and GFP-KASH4 overexpressing cells. GFP-KASH4–expressing cells have a ring formed around the nucleus. The VIFs' structure and organization do not change on disruption of LINC complex by GFP-KASH4 overexpression. (*D*) Vimentin filaments in cells expressing SS-GFP-KDEL or SS-HA-SUN1L KDEL.

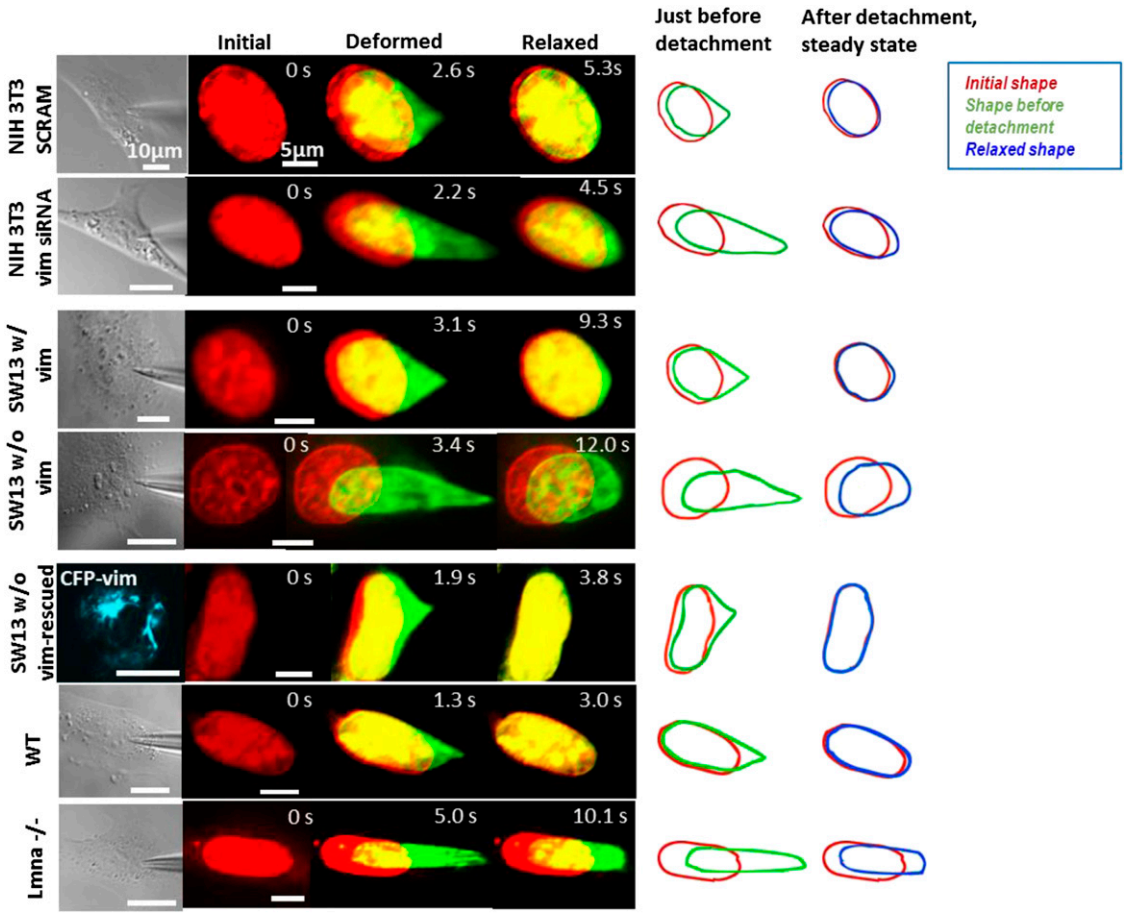

Fig. S7. Vimentin intermediate filaments and nuclear lamin A/C stiffen the nucleus and confine its position. Images of a typical NIH 3T3 cell initially (*Left*), overlay after forcing (*Center*), and overlay after detachment (*Right*). The nucleus was stained with SYTO 59 dye; the colors are to aid visualization (red, before forcing; green, deformed or relaxed) and correspond to the same dye. Montage shows characteristic behavior of the nucleus in the nuclear forcing experiment under different conditions. DIC images (left column) show the corresponding cell. The initial shape, the deformed shape just before detachment, and the relaxed (steady-state) shape after detachment are shown. Outlines of the initial nuclear shape (red) and the shape just before detachment (green) as well as the final relaxed shape (blue) are overlaid on the right to show the extent of deformation and relaxation of deformation. *Lmna*$^{-/-}$, MEFs lacking lamin A/C; NIH 3T3 SCRAM, NIH 3T3 cells transfected with scrambled siRNA; NIH 3T3 vim siRNA, NIH 3T3 cells transfected with vimentin siRNA; SW13 w/vim, SW13 cells containing vimentin; SW13 w/o vim, SW13 cells lacking vim; SW13 w/o vim vim-rescued, SW13 cells lacking vimentin rescued by transfection with CFP-vimentin; WT, wild-type MEFs.

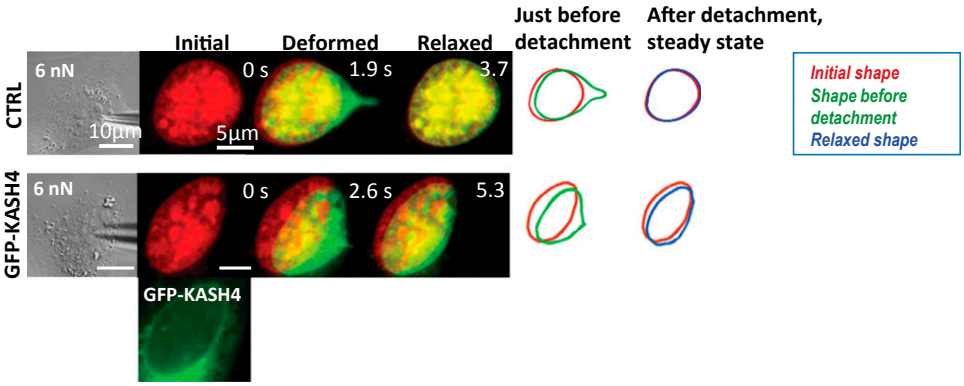

Fig. S8. Nuclear mechanics in NIH 3T3 fibroblasts expressing GFP-KASH4. Representative examples of nuclear manipulations in control and GFP-KASH4–expressing NIH 3T3 fibroblast cells. GFP-KASH4 can be seen to form a clear ring-like structure at the nuclear envelope (bottom). As shown in Table 1, only repositioning of the nucleus is affected by KASH4 expression.

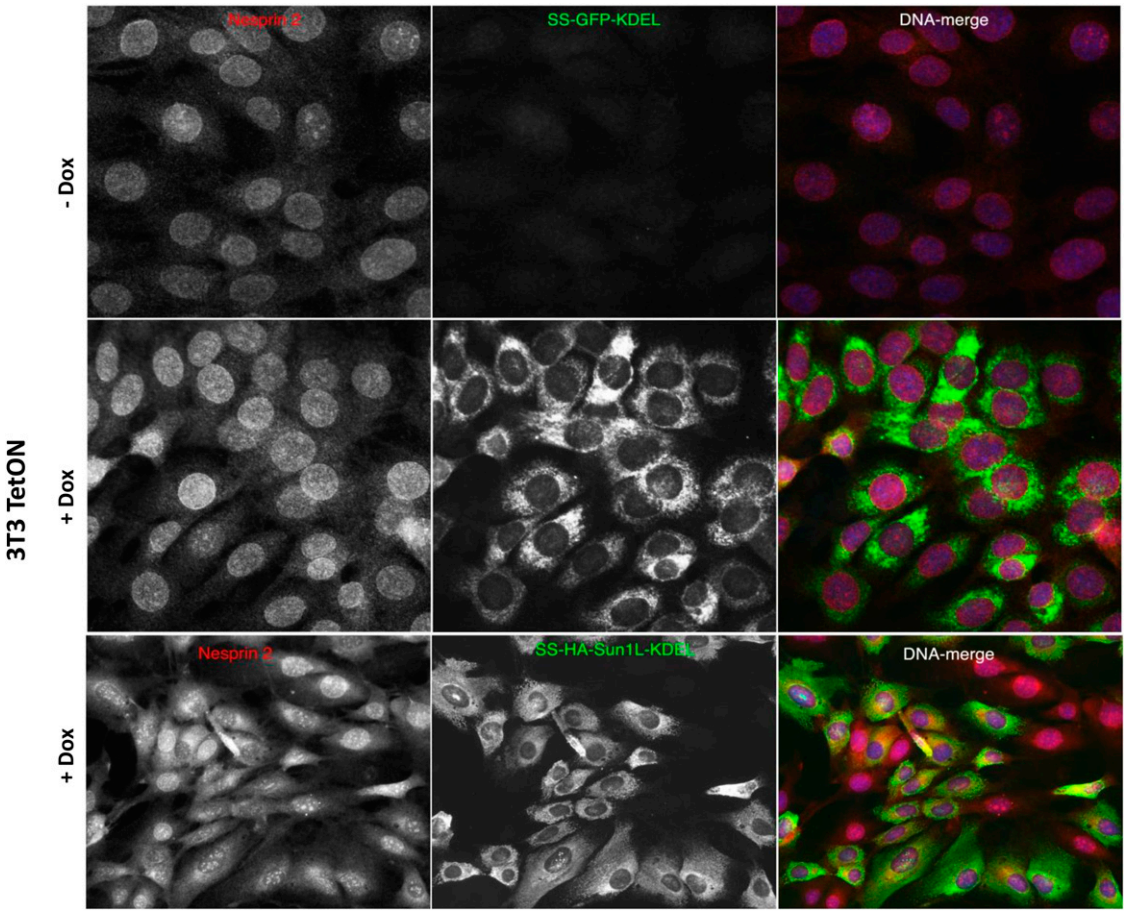

Fig. S9. (*Top*) 3T3 TetON pTight SS-GFP-KDEL cells, uninduced (−Dox) and induced with doxycycline (+Dox). There is Nesprin-2 staining at the nuclear membrane (left column) on inducing the GFP-KDEL protein. (*Bottom*) 3T3 TetON pTight SS-HA-Sun1L-KDEL cells. A loss of Nesprin-2 is observed in the Sun1L-KDEL in induced cells.

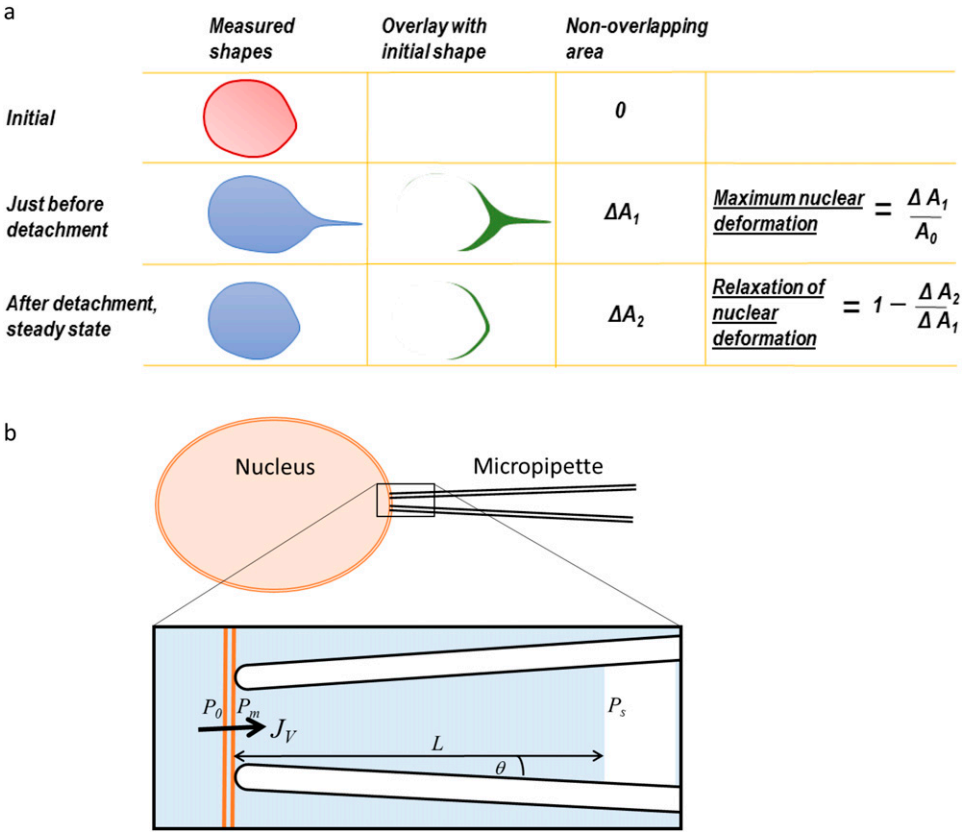

Fig. S10. (*A*) Schematic explaining the method for quantification of maximum nuclear deformation and relaxation of nuclear deformation. The deformed nuclear shape just before detachment from the micropipette tip was overlaid on the initial shape; the translation of the deformed nucleus was corrected for by aligning the back edges of the initial and deformed nuclear shape. The area that is not common between the two nuclei in the overlay was quantified (ΔA_1) and divided by the area of the initial nuclear shape (A_0) to get the maximum nuclear deformation. A similar procedure of overlay and alignment of the back edge was used to calculate the nonoverlapping area at steady state between the initial and the final nuclear shape on detachment from the tip; the nonoverlapping area $\Delta A_2/\Delta A_1$ is the unrecovered deformed area. (*B*) Schematic of micropipette pulling experiments showing the relevant pressures and parameters for a fluid mechanical analysis.

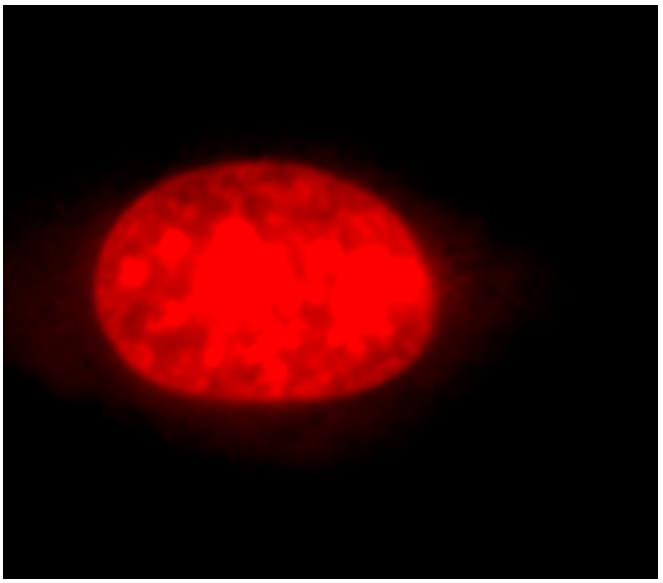

Movie S1. Nuclear forcing in a living, adherent cell. The SYTO 59-labeled NIH 3T3 fibroblast nucleus deformed and translated upon local forcing, and relaxed rapidly after detachment. The front and back edge are marked with blue asterisks.

Movie S1